JOURNAL OF GEOPHYSICAL RESEARCH, VOL. 112, D14305, doi:10.1029/2006JD007940, 2007

Regulation of H_2O and CO in tropical tropopause layer by the Madden-Julian oscillation

Sun Wong[1] and Andrew E. Dessler[1]

Received 21 August 2006; revised 20 February 2007; accepted 26 February 2007; published 20 July 2007.

[1] Impacts of the Madden-Julian oscillation (MJO) on the water vapor (H_2O) and carbon monoxide (CO) abundances in the tropical tropopause layer (TTL) are investigated using Aura Microwave Limb Sounder (MLS) data for November 2004 to May 2005. The effects of the eastward propagation of MJO on H_2O and CO abundances in the TTL are evident. Deep convection transports H_2O into the upper troposphere up to about the 355- to 365-K level. Around the 365- to 375-K level, a dry anomaly is collocated with a cold anomaly, which is above a warm anomaly located near the region of convection enhancement. Tropical mean H_2O at 375 K is regulated by the MJO through convection enhancement and is coherent with the local MJO-related temperature variation. The locations of dehydration follow the eastward propagation of convection enhancement, and its area extent depends on the phase of the MJO. Enhancement of deep convection associated with the MJO also injects CO from the lower troposphere to the TTL up to 375 K. However, tropical mean CO at 375 K responds instantaneously to the large injection event occurring over the African continent.

Citation: Wong, S., and A. E. Dessler (2007), Regulation of H_2O and CO in tropical tropopause layer by the Madden-Julian oscillation, *J. Geophys. Res.*, *112*, D14305, doi:10.1029/2006JD007940.

1. Introduction

[2] Understanding the physical and chemical processes that regulate the chemical composition of the upper troposphere and lower stratosphere (UT/LS) is an important goal of the scientific community. One particularly important but poorly studied area is the interaction between overshooting convection and large-scale processes occurring in the tropical tropopause layer (TTL), a transition region between the troposphere and stratosphere ($\sim$14–19 km, $\sim$355–400 K potential temperature) [*Folkins et al.*, 1999; *Sherwood and Dessler*, 2000, 2001; *Gettelman et al.*, 2002a, 2004]. *Sherwood and Dessler* [2001] showed that the observed H_2O and O_3 profiles can be reproduced by a model that incorporated overshooting convection. In subsequent papers, they also show that this model can explain the seasonal cycle of trace gases in the TTL [*Sherwood and Dessler*, 2003] and the abundance of water's isotopes [*Dessler and Sherwood*, 2003]. *Dessler* [2002] used measurements of O_3 and CO to estimate that about 60% of the mass crossing the 380 K surface is detrained above 370 K.

[3] Models that do not explicitly include overshooting deep convection [*Fueglistaler et al.*, 2004; *Read et al.*, 2004a; *Gettelman et al.*, 2002b; *Holton and Gettelman*, 2001] have shown that slow ascent of air parcels followed by rapid horizontal transport that brings air parcels through regions of cold temperatures (cold trap) in the TTL can also reproduce H_2O and ice fields compared to observations. The cold trap is identified as the region of coldest temperatures in the TTL, mainly over the western Pacific Ocean.

[4] Studying variations in tropical convective activity and the associated variations in chemical constituents provides a means to understand how deep convection affects the chemical composition of the UT/LS. One of the strongest variations in tropical convective activity is an eastward propagation of convection with a timescale of 30–60 days, known as the tropical intraseasonal oscillation or Madden-Julian oscillation (MJO) [*Madden and Julian*, 1971, 1972, 1994]. The MJO involves an interaction between large-scale tropical dynamical systems and convection, and its observed structure is well documented although the underlying mechanisms are still elusive [*Kiladis et al.*, 2005, and references therein].

[5] In general, regions of enhanced deep convection, represented by a reduction in outgoing longwave radiation (OLR), are observed moving eastward with anomalies in 200-hPa wind divergence with a timescale of 30–60 days. Deep convection transports water vapor as well as other chemical constituents from the lower troposphere to the upper troposphere [*Dessler*, 2002; *Pickering et al.*, 1996]. It also warms the troposphere by releasing latent heat. In the TTL, overshooting deep convection reduces the local temperature [*Sherwood et al.*, 2003; *Kuang and Bretherton*, 2004; *Wu et al.*, 2006; *Holloway and Neelin*, 2006]. Convection can affect H_2O through either direct injection of moist or dry air or indirectly by cooling the TTL, which leads to loss of H_2O by condensation and precipitation. Consequently, it is natural to expect that H_2O and other

[1]Department of Atmospheric Sciences, Texas A&M University, College Station, Texas, USA.

0148-0227/07/2006JD007940$09.00

constituents may be influenced by the MJO through the eastward migration of convection enhancement.

[6] *Mote et al.* [2000] and *Sassi et al.* [2002] investigated the influence of MJO on H_2O in the UT/LS region using the Microwave Limb Sounder (MLS) [*Read et al.*, 2004b] on the Upper Atmosphere Research Satellite [e.g., *Dessler et al.*, 1998]. They found that eastward movements of H_2O and relative humidity anomalies at 215 and 100 hPa were coherent with the movements of the deep convective activity and temperature anomalies in the Eastern Hemisphere (roughly around 60°–180°E). Convection associated with the MJO moistens at 146 hPa and dries at 100 hPa [*Mote et al.*, 2000].

[7] In this paper, we study H_2O and CO in the TTL and investigate how the tropical mean H_2O and CO entering the lower stratosphere are regulated by the MJO. In the TTL, both H_2O and CO are influenced by deep convection, which transports air from the lower troposphere into the UT/LS. However, the ability of H_2O to be removed by condensation followed by precipitation makes its abundance sensitive to temperature variations, while CO is not. Comparing how these two constituents respond to variations in convective activity and temperature therefore provides information about transport and dehydration processes in the TTL.

2. Data Resources

[8] We analyze intraseasonal variations of H_2O and CO volume mixing ratios from Aura MLS level-2 data (version 1.51) for the period November 2004 to May 2005, a season that includes the main biomass burning season of the equatorial Africa [*Duncan et al.*, 2003] and TTL is colder than the rest of the year. H_2O is retrieved with a vertical resolution of about 3 km in the UT/LS and with an expected accuracy of 10% [*Livesey et al.*, 2005]. CO is retrieved with a vertical resolution of about 4.5 km in the UT/LS. CO concentration values at 215 hPa have a large positive bias ($\sim 2\times$ larger than values from GEOS-CHEM model) [*Livesey et al.*, 2005]. As a result, we analyze variations in CO concentrations in the UT/LS rather than the exact magnitude of the changes. The Aura MLS data have been used to study the seasonal variations of CO in the UT/LS [*Schoeberl et al.*, 2006].

[9] The daily MLS H_2O and CO data are averaged into $5° \times 5°$ grid boxes. The original data are given at pressure levels of 316.2, 215.4, 146.8, 100, and 68.1 hPa in the UT/LS, corresponding to typical potential temperature levels of 340–345, 348–351, 354–359, 366–375, and 420–430 K, respectively, in the deep tropics (the ranges span the longitudinal variations of potential temperatures of the corresponding pressure levels). In this study, we have linearly interpolated the data vertically onto potential temperature surfaces of 345, 355, 365, and 375 K, using temperatures from NCEP/NCAR reanalysis data [*Kalnay et al.*, 1996]. Analyzing short-term transport on isentropic levels can eliminate the effects of large-scale adiabatic warming/cooling by deep convection (for example, lifting or sinking of isentropes over deep convection) and can obtain results that are relevant to diabatic effects related to convective detrainments.

[10] Daily outgoing longwave radiation (OLR in watt per square meter) data for the period of November 2004 to May 2005 are used as a proxy for tropical convective activity. The OLR data are from the National Oceanic and Atmospheric Administration (NOAA) interpolated OLR data set [*Liebmann and Smith*, 1996].

Table 1. MJO Phases Used in This Study and Their Corresponding Locations of Velocity Divergence at 200 hPa in the First EEOF

P1	P2	P3	P4	P5	P6
80°E	120°E	140°E	160°E	40°W	20°E

[11] In order to study the impacts of the MJO, MJO indices were obtained from the NOAA/Climate Prediction Center (CPC) Web site (http://www.cpc.noaa.gov/product/precip/CWlink/daily_mjo_index/mjo_index.shtml). The indices are computed by applying extended empirical orthogonal function (EEOF) analysis [*Weare and Nasstrom*, 1982] to pentad velocity potential at 200 hPa with two successive pentads separated by a time lag of 5 days. We utilize six indices from the CPC data to represent six phases of the MJO and name them P1 to P6, respectively. Each index is associated with a pentad of the first EEOF that represents a phase of the MJO in which the negative velocity potential anomalies (divergence of horizontal winds) at 200 hPa propagate to a certain longitude of the tropical band. The P1 phase represents a pentad of the first EEOF with divergence at 200 hPa located around 80°E over the equator, the P2 phase has the divergence shifted to about 120°E after about 10 days, the P3 phase to about 140°E after about another 5 days, the P4 phase to about 160°E, the P5 phase to about 40°W, and the P6 phase to about 20°E. We summarize the location of wind divergence at 200 hPa in the first EEOF for each phase used in this study in Table 1. Since the phase speed of MJO propagation in the Eastern Hemisphere is slower than that in the Western Hemisphere [*Madden and Julian*, 1994; *Kiladis et al.*, 2005, and references therein], we have more indices for the phases of the MJO in the Eastern Hemisphere.

[12] In this study, we applied 5-day averages for all time series for consistency with the MJO pentads. This averaging process reduces the noise in MLS data while retaining the MJO signals.

3. Composite Analysis

3.1. The MJO Effect on TTL Temperatures

[13] Figure 1 shows a Hovmöller diagram of the OLR averaged between 10°S and 10°N for November 2004–May 2005. *Kiladis et al.* [2005] showed the geographical daily standard deviation of MJO-filtered OLR for the period 1979–2004 (their Figure 1), and the main variability of OLR is located at 10°S–10°N. We also test the OLR variability by averaging over a larger latitude range of 15°S–15°N, and the results do not change significantly from that shown in Figure 1. Eastward propagation of deep convection (typically with OLR < 220 W m^{-2}) is evident over the Indo/Pacific Ocean and western Pacific Ocean (60°–180°E). There are also deep convections appearing over the eastern South America, the Atlantic Ocean around 60°–80°W, and the African continent (0°–20°E). Over 40°–60°E and 80°–120°W, there is almost no deep convection.

[14] For each MJO index, we calculate the composite OLR anomaly by averaging the daily OLR between 10°S

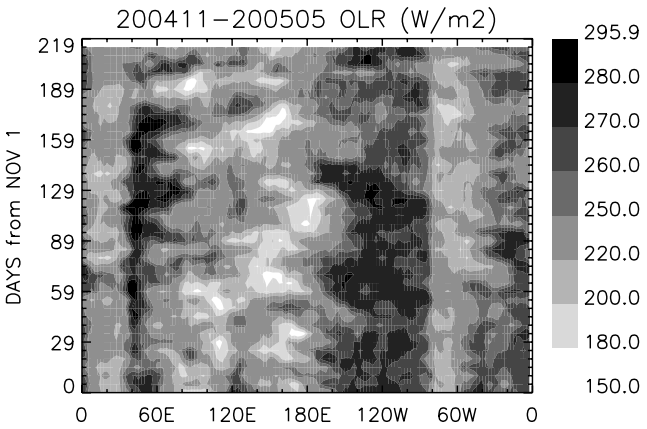

Figure 1. Outgoing longwave radiation in watt per square meter for November 2004 to May 2005 averaged between 10°S and 10°N.

and 10°N from days with that MJO index less than −0.5 and by subtracting the average daily OLR for the whole period of November 2004–May 2005. Negative (positive) anomalies mean that convection is enhanced (suppressed) compared to the period averages. Figure 2 shows the composite OLR anomalies (as a percentage departure from the period-average OLR) for the six MJO indices.

[15] From the first index to the fourth one (P1–P4), enhancement of convection moves from the Indo/Pacific Ocean (60°–120°E) eastward to the western Pacific Ocean about 120°–180°E. There is suppression of deep convection on the east or west flank of the region of convection enhancement. This suppression of convection is associated with the downward motion adjacent to the region of convection enhancement [*Kiladis et al.*, 2005 (their Figure 6)]. For the fifth index (P5), enhancement of convection over the western Pacific Ocean becomes insignificant, and significant enhancement of convection occurs near the eastern coast of South America (around 40°–60°W) and the African continent (0°–20°E). Meanwhile, strong suppression of convection occurs over the Indo/Pacific Ocean (60°–120°E). For the sixth index (P6), convection enhancement over the eastern coast of South America and the African continent becomes marginally significant, and area of suppression of convection shifts to about 120°–180°E. Note also that the MJO-related convection enhancement is stronger in the Indian and Pacific oceans (P1–P4) than in South America and Africa (P5 and P6).

[16] Figure 3 shows the composites of tropical mean (10°S–10°N) temperature anomalies on potential tempera-

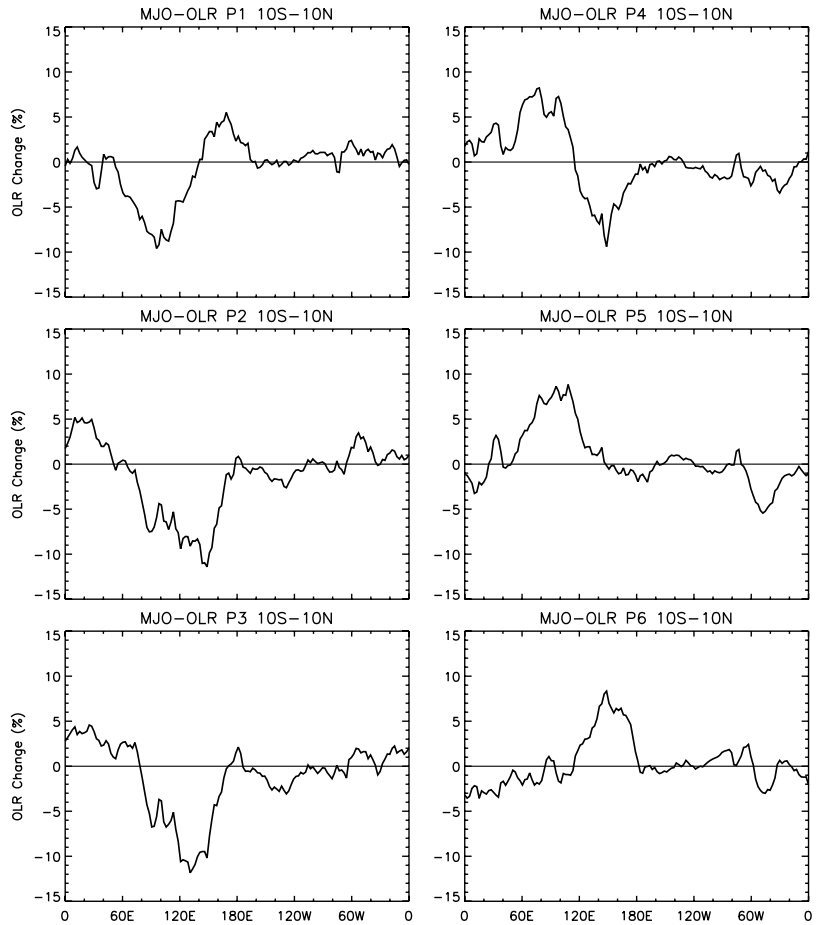

Figure 2. Zonal variation of anomalies in outgoing longwave radiation (in watt per square meter) averaged between 10°S and 10°N for phases of the MJO corresponding to different pentads (see text). The anomalies are departures from the mean values for November 2004–May 2005.

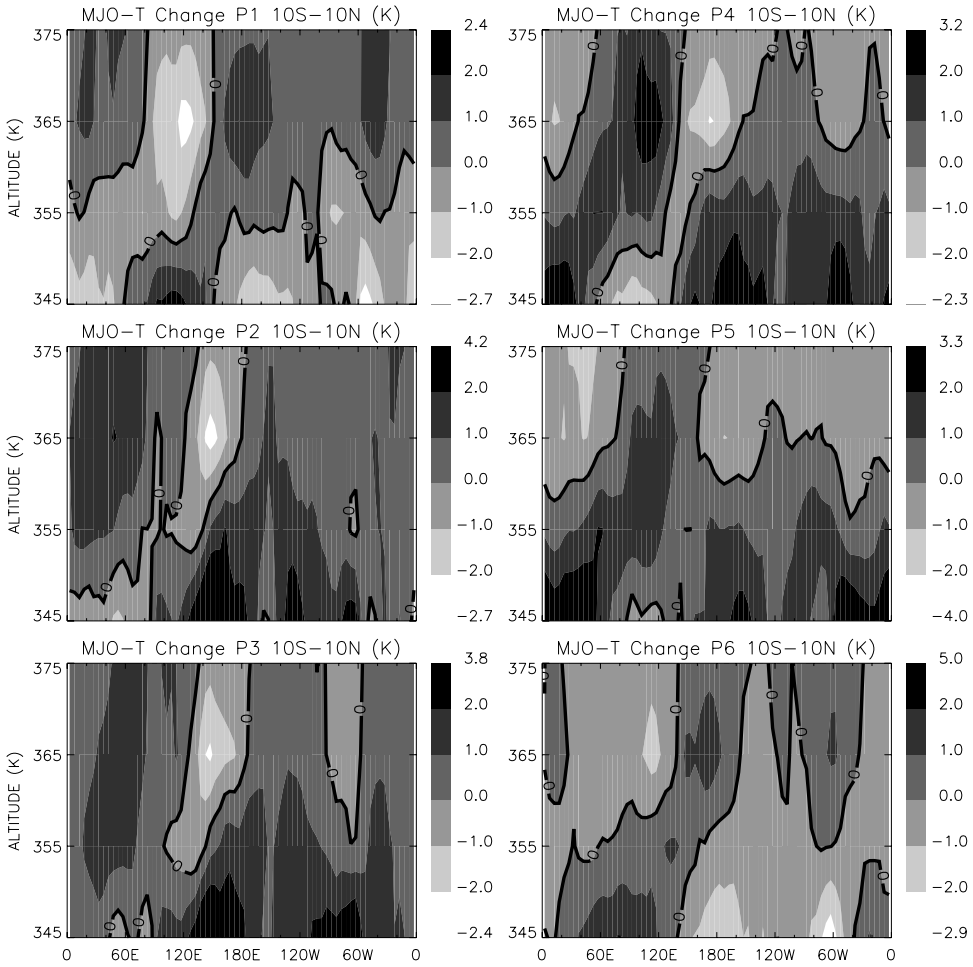

Figure 3. Longitude-altitude distribution of NCEP temperature anomalies (in Kelvin) averaged between 10°S and 10°N for phases of the MJO corresponding to different pentads. The anomalies are departures from the mean values for November 2004–May 2005.

ture altitudes of 345–375 K for different phases of MJO. For P1–P4, a warm anomaly at 345 K is located close to the longitude of convection enhancement. Clearly, the warm anomaly propagates eastward from Indian to Pacific Ocean with the convection enhancement. This warm anomaly is associated with the balance between convective heating and adiabatic cooling in the middle-upper troposphere and it tilts eastward in the vertical, consistent with the upward group velocity of a forced gravity wave response to the eastward moving MJO and the associated convective heating [*Gill*, 1980; *Kiladis et al.*, 2005; *Randel et al.*, 2003; Son S. W. and Lee S., Intraseasonal variability of the zonal mean tropical tropopause height, submitted to *Journal of the Atmospheric Sciences*, 2006, hereinafter referred to as Son and Lee, submitted manuscript, 2006]. Directly above the warm anomaly is a cold anomaly due to adiabatic lofting caused by convective heating below [*Holloway and Neelin*, 2006; *Sherwood and Dessler*, 2003]. The cold anomaly maximizes in the range of 365–375 K. This vertical structure is consistent with previous findings using either reanalysis data [*Kiladis et al.*, 2005] or GPS temperature sounding [*Randel et al.*, 2003].

[17] From P4 to P6, the warm anomaly at 345–355 K over the Pacific Ocean at 180°E is gradually replaced by a cold anomaly when the local enhancement of deep convection decreases. Over the eastern coast of South America (40°–60°W) and the African continent (0°–20°E), warm anomalies arise with the local enhancement in convection (P4 and P5). There are always cold anomalies located above the warm anomalies.

[18] For P5 and P6, convection is enhanced mainly over the eastern South America (40°–60°W) and Africa (0°–20°E) and is suppressed over the Indo/Pacific Ocean (60°–120°E in P5) or western Pacific Ocean (120°–180°E in P6). One sees in P5 that cold anomalies (warm anomalies) occupy in regions throughout the equatorial band at 365–375 K (345–355 K) except near the region where convection is suppressed.

[19] In conclusion, the location and size of TTL temperature anomalies caused by deep convection depend on the phase of the MJO. In P1–P2, when the convection is enhanced over the western Pacific Ocean, the associated cold (warm) anomaly at 365–375 K (345–355 K) is located in a limited area; in the phases when the convection enhancement propagates to Atlantic Ocean and Africa (P5 and P6), the corresponding temperature anomalies occupy larger area of the tropical band. This temporal variation in the spatial distribution of the cold anomalies at 365–375 K

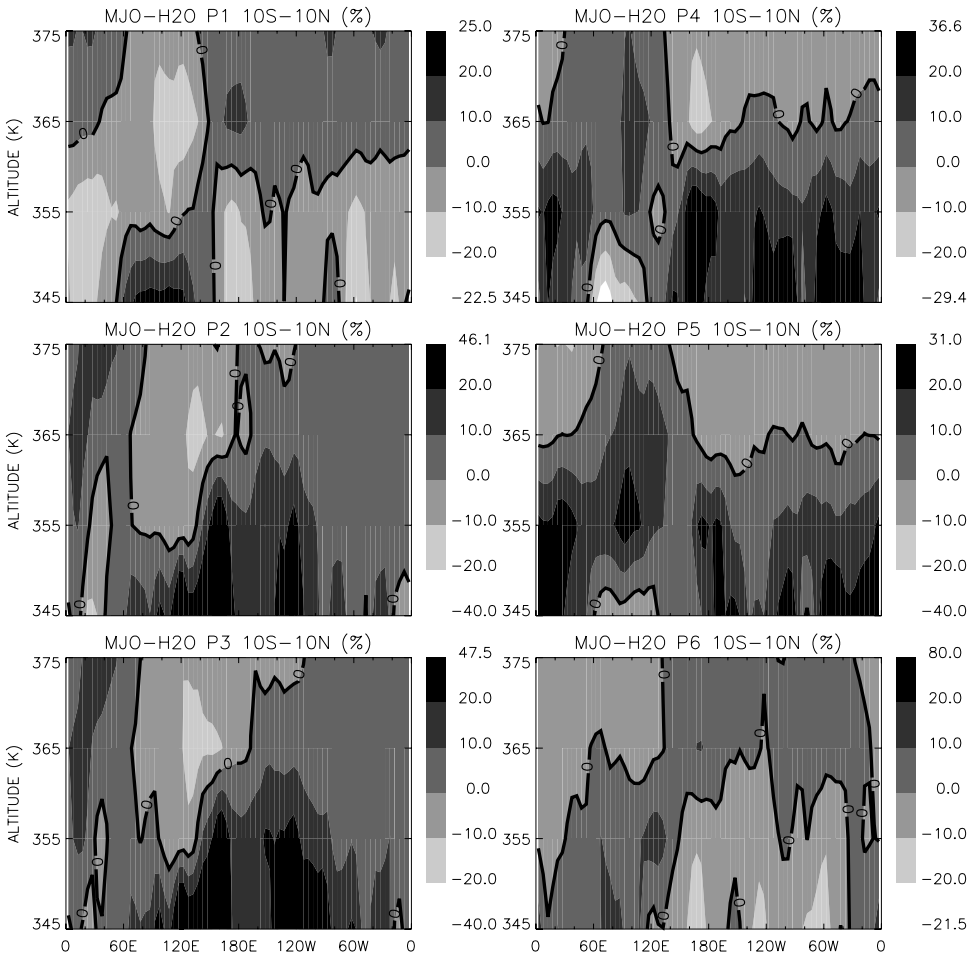

Figure 4. Similar to Figure 3 but for Aura MLS H_2O concentration anomalies. The anomalies are expressed as percentage change from the mean values for November 2004–May 2005.

is relevant to how dehydration depends on the phase of the MJO through the migration of convection enhancement.

3.2. The MJO Effects on TTL H_2O and CO

[20] As we did for temperature, we construct the MJO composite of anomalies for H_2O and CO concentrations between 10°S and 10°N. Figure 4 shows plots similar to Figure 3 but for H_2O. The significant anomalies are about ±10–20% at 365 K and 20–50% at 345 K, consistent with the previously published ranges of anomalies for the MJO [*Mote et al.*, 2000]. These H_2O anomalies are also comparable to the seasonal variations of the zonal mean water vapor at the corresponding levels [*Read et al.*, 2004a]. In general, the H_2O anomalies resemble the temperature anomalies, with positive (negative) H_2O anomalies associated with warm (cold) temperature anomalies. However, there are differences in the details. The H_2O anomalies at 345–355 K are not exactly collocated with the corresponding temperature anomalies. Over regions where convection is enhanced, H_2O is transported from the lower to the upper troposphere. Therefore increases in H_2O are more closely collocated with enhancements in convection. Temperature anomalies are the result of the balance between diabatic and adiabatic heating and the Kelvin-wave response that tilts the temperature anomalies eastward [*Randel et al.*, 2003]; therefore they do not exactly line up with the H_2O and OLR anomalies.

[21] At 365–375 K, as was the case of the cold anomalies, the area extent of the dry anomalies depends on the phase of the MJO. In P1, when the convection is enhanced over the western Pacific Ocean, the associated dry anomaly at 365–375 K is located in a limited area; in the phases when the convection enhancement propagates to Atlantic Ocean and Africa (P5), the corresponding H_2O anomalies occupy larger area of the tropical band.

[22] Despite a clear connection between negative H_2O anomalies with cold temperature anomalies at 365–375 K, the exact mechanisms connecting these fields are still unclear. We cannot determine whether it is the synoptic-scale temperature field, as suggested by *Holton and Gettelman* [2001], or the unresolved temperature fluctuations, as suggested by *Potter and Holton* [1995], or the convective dehydration, as suggested by *Sherwood and Dessler* [2001]. Clearly, more work on this important question is required.

[23] Figure 5 shows the composites of anomalies for tropical CO. We note that while CO is photochemically active, on the timescale of interest here (a few weeks), CO in the TTL is essentially conserved. *Dessler* [2002] estimated the lifetime of CO with respect to production and loss to be a few thousand and a hundred days, respectively.

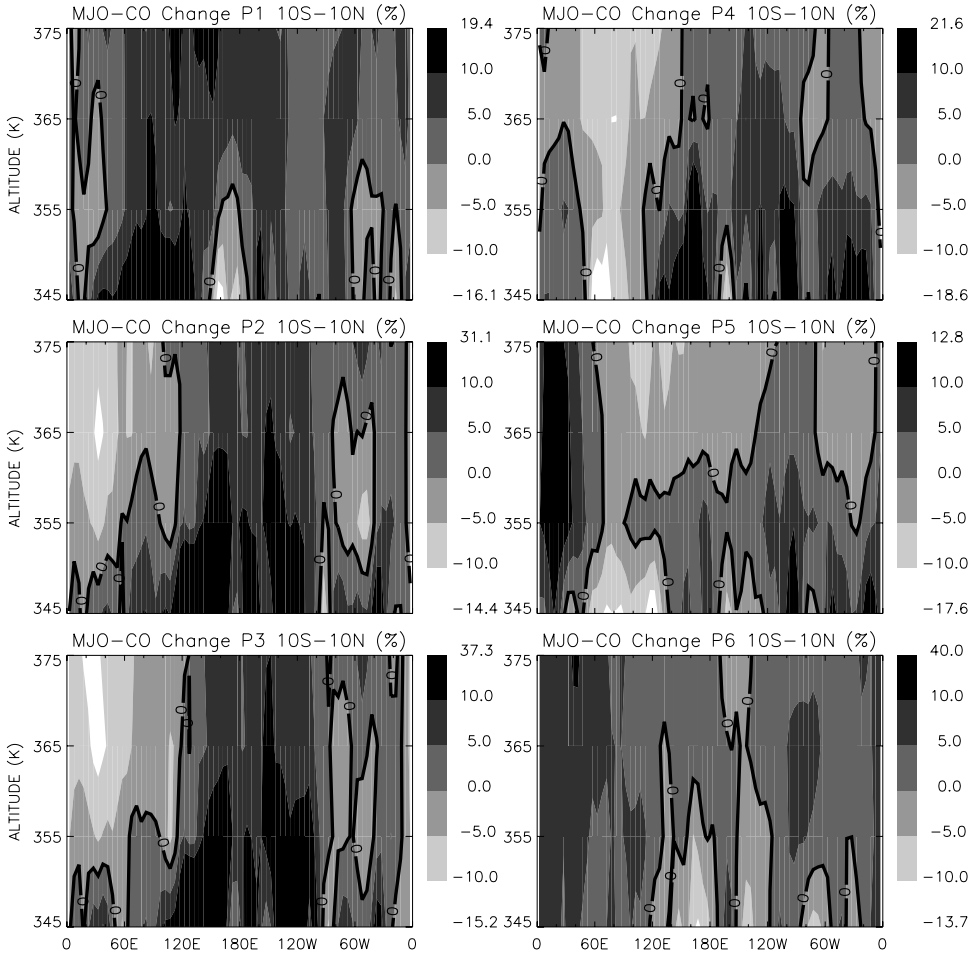

Figure 5. Similar to Figure 3 but for Aura MLS CO concentration anomalies. The anomalies are expressed as percentage change from the mean values for November 2004–May 2005.

Therefore we can neglect the effects of chemistry on CO anomalies in this analysis.

[24] Positive (negative) anomalies mean that the CO concentrations are higher (lower) than the period average. The source of CO in the TTL is mainly from detrainment of CO-rich air from convection. Consequently, positive CO anomalies at 345–355 K are collocated with the area of enhanced convection, and they therefore tend to line up with the moist anomalies. Moreover, the positive CO anomalies associated with the convection enhancement extend to around 375 K. Finally, the CO enhancement propagates with the enhancement of convection along the tropical band.

4. Correlation Analysis

4.1. Variations of H_2O and CO in the TTL Associated With the MJO

[25] We investigate the variations of H_2O and CO concentrations at 365 K averaged in the latitudinal band of 10°S–10°N. In order to remove long-term variability, we assume that the long-term variations are sinusoidal with a period of 1 year. The sinusoidal amplitude and phase at each location are obtained by fitting the data from November 2004 to May 2005. The anomalies are the residues of the time series after subtraction of the long-term variations.

[26] Figure 6 shows the Hovmöller diagrams of the variations of H_2O and CO anomalies at 365 K. There is correspondence between deep convection shown in Figure 1 and dry (negative) anomalies shown in the top panel of Figure 6. The eastward propagation of dry and wet anomalies is evident, indicating that the MJO modulates H_2O in TTL through the eastward migration of convection enhancement.

[27] For CO, there is also evident eastward propagation of positive and negative anomalies, showing that convection enhancement associated with the MJO injects lower tropospheric CO into the TTL (see Figure 5). The three dominant maxima (in the lower panel of Figure 6) are located over 100°–140°E (Indonesia) around days 0–10 (early November 2004) and over 0°–20°E (Africa) around days 119–139 (late February–early March 2005) and days 170–189 (late April–early May), which correspond to enhancement of local convective activity related to the MJO (see Figure 1).

4.2. Timescales of the Intraseasonal Variations

[28] Time-lag correlations of the variations of H_2O and CO anomalies in the TTL with their corresponding tropical mean concentrations at 375 K can further relate the intraseasonal variations of the constituents to the MJO. The tropical mean is defined as the zonally averaged H_2O and

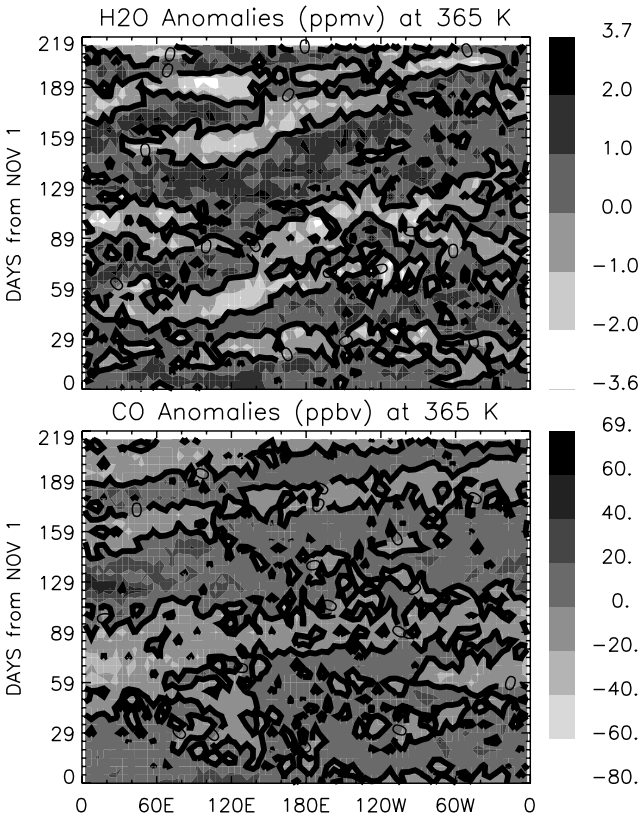

Figure 6. H_2O (in parts per million by volume) and CO (in parts per billion by volume) concentration anomalies at 365 K for November 2004–May 2005. The thick solid lines are zero lines.

CO concentrations in the latitudinal band of 10°S–10°N. We compute time-lead correlations between the tropical mean constituent concentration anomalies at 375 K and the concentration anomalies at each longitude and altitude averaged between 10°S and 10°N for the period of November 2004 to May 2005.

$$\mathrm{corr}(\lambda, z, \tau) = \frac{\sum_n \chi(\lambda, z, n-\tau) \cdot \chi_{\mathrm{trp}}(n)}{\sqrt{\sum_n [\chi(\lambda, z, n)]^2} \cdot \sqrt{\sum_n [\chi_{\mathrm{trp}}(n)]^2}}$$

where $\chi(\lambda, z, n)$ represents the constituent concentration anomaly in the tropics at a longitude-altitude grid (λ, z) on the nth day between 1 November 2004 and 31 May 2005, $\chi_{\mathrm{trp}}(n)$ represents the concentration anomaly of the tropical mean on the nth day at 375 K, and τ represents a time lag. Such correlations reveal the altitude-longitude structure of the anomalies, which is associated with the tropical mean variation at 375 K at a time leading the tropical mean. This is similar to the approach taken by Son and Lee [submitted manuscript, 2006] to investigate the regulation of temperature in the TTL. We estimate the statistical significance using Student's t test, with the degree of freedom adjusted by the autocorrelations of the time series [*Bretherton et al.*, 1999]. For Figure 7 and Figure 9, correlations over the 90% confidence level are shown in dotted lines. For Figure 8 and Figure 10, we include the maximum requirements for correlations at the 90% confidence level as the horizontal dotted lines so that correlations beyond these values are guaranteed to be at least 90% confidence.

[29] Figure 7 shows the time-lead correlations for the tropical mean H_2O concentration anomaly at 375 K for different time leads (from 30 to 0 days). Regions of positive correlations mean that the local decrease in H_2O leads the decrease in the tropical mean H_2O by the specified time lead. The top panel (time lead of 30 days) shows that, 30 days before the zonal mean H_2O decreases, dehydration occurs mainly over the western Pacific Ocean around 365–375 K. At time leads of 15 and 10 days (the second and third panels), the area of dehydration at 365–375 K propagates eastward to 140°–180°E. Moreover, positive correlations appear over the eastern Pacific Ocean, South America, Atlantic Ocean, and Africa (120°W–20°E).

[30] In Figure 4, we see that the negative anomaly of H_2O at 365–375 K associated with the MJO is mainly located over the Indo/Pacific Ocean in P1, and it propagates toward the western Pacific Ocean from P1 to P5. Meanwhile, negative anomalies at 365–375 K also appear over the eastern Pacific Ocean, South America, Atlantic Ocean, and Africa (120°W–20°E). This propagation pattern of the MJO-associated negative anomalies of H_2O shown in Figure 4 is consistent with that of the positive correlations shown in Figure 7. Moreover, the time-lag correlation between the MJO indices representing P1 and P5 (not shown) shows a peak at 15–20 days, meaning that the time span between P1 and P5 is approximately 15–20 days. This time span is consistent with the time span from the top panel in Figure 7 to the second and third panels in Figure 7 (about 15–20 days). This suggests that the time-lag correlations shown in Figure 7 are probably caused by the MJO.

[31] We further investigate the relationship between the MJO and the TTL H_2O by computing the time-lag correlations between three MJO indices (P2, P4, and P5) and the tropical mean H_2O anomaly at 365 K (Figure 8). The peak of the correlation for P2 precedes the variation of the tropical mean H_2O by about 30–35 days, consistent with the top panel of Figure 7 that shows dehydration over the western Pacific Ocean for this time lead. This connects the top panel of Figure 7 with the P2 in Figure 4. The peak of the correlation for P4 (P5) precedes the variation of the tropical mean H_2O by 15 (10) days. This means that the correlation patterns with time leads of 10 and 15 days in Figure 7 correspond to the phases of the MJO at or between P4 and P5. The multiple peaks in Figure 8 for each MJO index realize the quasiperiodicity of the MJO. The time span between the peaks varies in the range of 30–45 days, within the range of the known MJO period of about 30–60 days. The above discussion and Figures 3 and 4 illustrate that the MJO can modulate the TTL temperature and H_2O by the modulation of convection.

[32] On the other hand, CO is not sensitive to local temperature variations as H_2O is. This can be seen in Figure 9, which is the same plot as Figure 7, but for CO. Regions of positive correlations mean that the local increase in CO concentrations leads the increase in the tropical mean by the specified time lead. The correlation at the time lead of 25 days (the top panel) shows that the tropical mean concentration variations are mainly related to the CO concentration variation over the African continent (0°–20°E). For the time

leads of 15 to 0 days, the large positive correlations over the African continent extend their area and cover all the TTL area in the 0-day plot (the bottom panel).

[33] The large correlation over the African continent corresponds to the injection of CO from the lower troposphere during the phase of MJO when convection is enhanced over the African continent (Figure 5, P5–P6). This also corresponds to a particular event occurring in February–March (Figure 6, around days 120–139 over 0°–20°E). Therefore CO variation in the 375-K level is dominated, at least during this period, by the injection of large amount of CO over the African continent.

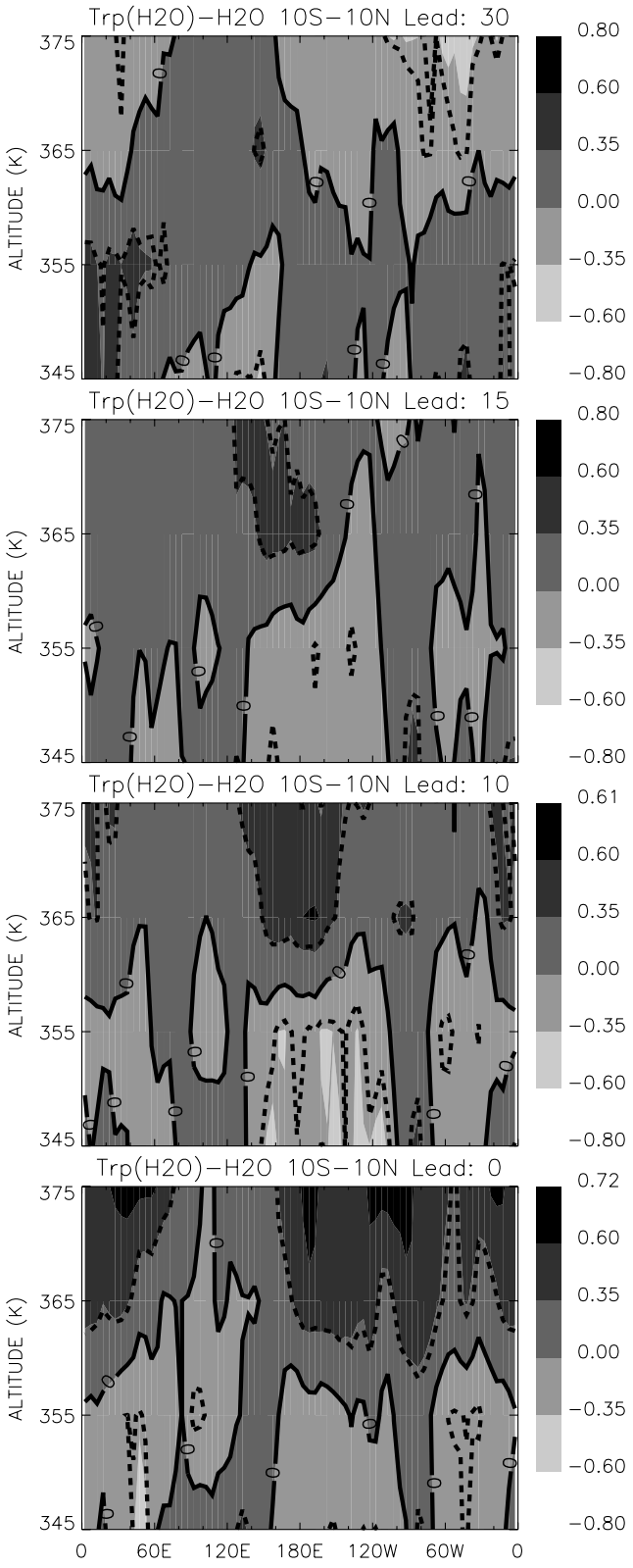

Figure 7. Longitude-altitude distribution of time-lead correlations between the 10°S- and 10°N-averaged Aura MLS H_2O concentration anomalies and the tropical mean H_2O concentration anomaly at 375 K for November 2004–May 2005. The tropical mean is defined as the H_2O concentrations averaged over all longitudes and latitudes for 10°S–10°N. The solid lines are zero contours, and the dashed lines show the 90% confidence levels of the correlations. The time leads are 30, 15, 10, and 0 days, respectively.

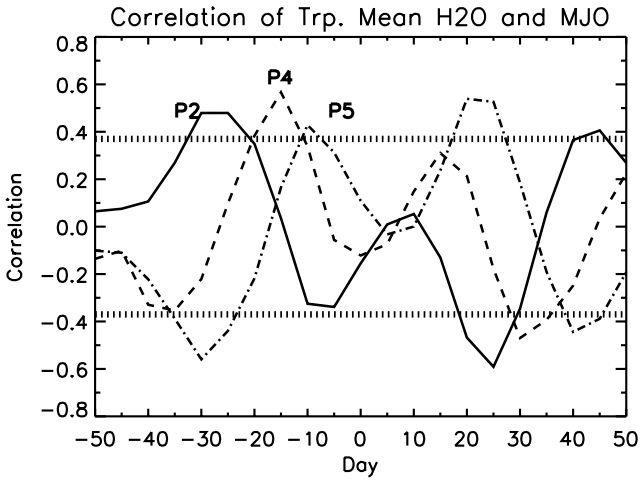

Figure 8. Correlations between the tropical mean H_2O concentration anomaly at 365 K and the three MJO indices for November 2004–May 2005. The solid line is for P2, the dashed line is for P4, and the dash-dotted line is for P5. The dotted lines are the maximum 90% confidence level. The peak of each MJO index preceding the tropical mean H_2O variation is marked by the corresponding phase label.

4.3. Zonal Responses to Regional Variations

[34] Because the intraseasonal variations of tropical mean H_2O and CO at 375 K are related with time lags to regional variations of the two constituents (Figures 7 and 9) in the TTL, we compute the time-lag correlations between the tropical mean concentration anomalies and the selected regional mean anomalies at 365 K. For H_2O, we choose a region of 100°–120°E and 10°S–10°N, which covers the tropical warm pool area over the western Pacific Ocean, for the regional mean. For CO, we choose a region of 5°–45°E and 10°S–10°N, which covers the tropical African continent. Figure 10 shows the time-lag correlations for the average anomalies of the two constituents.

[35] For H_2O, the tropical mean variation is significantly correlated with the variation over the western Pacific Ocean for a time lag of about −35 days (consistent with Figure 7). The peaks of the correlation curve are also close to (up to

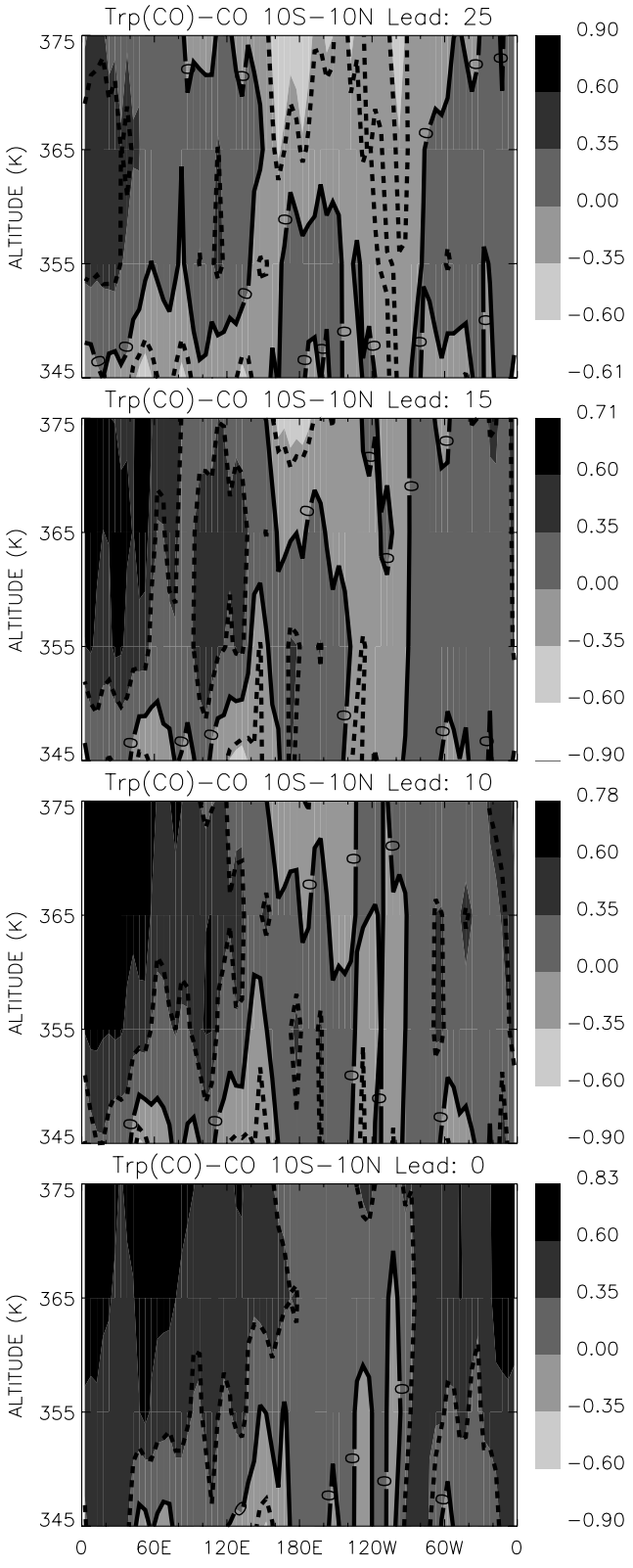

Figure 9. Similar to Figure 7 but for time-lead correlations between the 10°S- and 10°N-averaged Aura MLS CO concentrations and the tropical mean CO concentrations at 375 K. The time leads are 20, 15, 10, and 0 days, respectively.

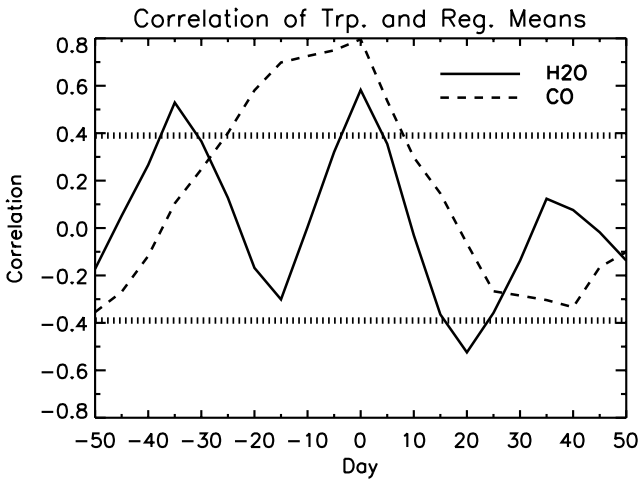

Figure 10. Correlations between the regional averaged and the tropical mean concentration anomalies for Aura MLS H_2O (solid line) and CO (dashed line) at 365 K for November 2004–May 2005. For H_2O, the regional average is taken over the western Pacific (10°S–10°N, 100°–140°E). For CO, the regional average is taken over the African continent (10°S–10°N, 5°–45°E). The dotted lines are the maximum 90% confidence level.

about 0–10 days of difference) those of the correlation curve between the tropical mean H_2O concentration anomaly and the MJO index P2 (Figure 8). Therefore the regional dehydration over the western Pacific Ocean 30 days preceding the decrease of the tropical mean H_2O is related to the phase of the MJO represented by P2.

[36] For CO, the correlation curve exhibits a rather flat top from about −15 to 0 days. The variation of the tropical mean CO is highly correlated with the regional CO over Africa for a time span of about 15 days. This is consistent with the fact that the injection of CO over Africa dominates the variation of CO in the TTL. The relatively flat correlation curve indicates that the injection of CO occurs for a relatively long time span. This can be clearly seen from the Hovmöller diagram (the lower panel of Figure 6) that the maximum around day 129 over 0°–20°E covers several weeks. The correlation curve drops with a timescale of about 0.5 month after day 0, and the tropical mean CO concentration becomes decoupled from the regional CO concentrations over the African continent after the injection event.

5. Conclusions and Discussion

[37] Analysis of Aura MLS H_2O and CO measurements during different phases of the MJO shows the impacts of the MJO on the chemical composition of the tropical tropopause layer (TTL). Convection enhancement associated with the MJO influences H_2O and CO in different ways, and its impacts reach up to the tropopause.

[38] For H_2O, increases are seen in the upper troposphere over regions where convection is enhanced by the MJO. This occurs because moisture is directly brought up to the lower part of the TTL by the updrafts of deep convection. Warm anomalies are located nearby although not exactly coincident with the H_2O. Drier air is collocated with cold

temperature anomalies at 365–375 K, which are located above the warm anomalies.

[39] The variation of the tropical mean H_2O concentration at 375 K is also shown to be regulated by the MJO. The region of dehydration propagates with the enhancement of deep convection eastward along the tropical band. Therefore dehydration can occur in regions remote from the western tropical Pacific Ocean, depending on the phase of the MJO.

[40] Enhancement in convection can inject CO from the lower troposphere into the TTL up to the 375-K level. CO anomalies in the TTL migrate eastward with the MJO-related convection enhancement. The variation of the tropical mean CO at 375 K is mainly controlled by the occurrence of convection over Africa. Large CO injection events over Africa are seen in February–March, and these events dominate the tropical mean CO variation at 375 K.

[41] There are still a lot of remaining issues. For large-scale pattern, the pair of cyclonic circulations located eastward of the convective outflow (or wind divergence) at 200 hPa may bring in subtropical-extratropical air mass into the deep tropics. It will be interesting to investigate how the intrusion from the extratropics is realized in the H_2O [e.g., *Waugh*, 2004] and CO budgets related to the MJO. Our study uses data averaged over grid boxes of large area; therefore it only reveals the large-scale relationships between convection, temperature, and H_2O and CO concentrations. Since deep convection occurs on a spatial scale much smaller than the one being considered in this study, we still do not know the details of the smaller-scale processes and what role they play in the large-scale phenomena observed in this study. Moreover, we have not diagnosed the mechanism of dehydration in the TTL. Future investigation of ice and relative humidity fields in the conceptual frame of the structure of the MJO may give insights into this important process. The 3- to 4-K systematic warm bias of NCEP temperatures in the UT/LS may also cause a bias in the location of the isentropes being used in this study.

[42] Finally, this study only investigates data for November 2004–May 2005. It is known that the MJO has significant seasonal and interannual variability. For example, the variability in temperatures and H_2O caused by the MJO in the UT/LS was larger in December–May during 1991–1993 [*Mote et al.*, 2000]. Investigation for the seasonal and interannual variation in the MJO effects on the TTL H_2O and CO in other years will be a necessary task for future study.

[43] **Acknowledgments.** We thank the Aura Science Team for the MLS level-2 data of H_2O and CO, Kenneth Bowman and Rong Fu of Georgia Tech., Andrew Gettelman of NCAR, Mark Filipiak of the University of Edinburgh, Qing Liang of GSFC, and three anonymous reviewers for their comments and discussion. This work was supported by NASA Aura validation grant NNG06GF96G and NASA EOS/IDS grant NNG04GH67G, both to Texas A&M University.

References

Bretherton, C. S., M. Widmann, V. P. Dymnikov, J. M. Wallace, and I. Bladé (1999), The effective number of spatial degree of freedom of a time-varying field, *J. Clim.*, *12*, 1990–2009.

Dessler, A. E. (2002), The effect of deep, tropical convection on the tropical tropopause layer, *J. Geophys. Res.*, *107*(D3), 4033, doi:10.1029/2001JD000511.

Dessler, A. E., M. D. Burrage, J.-U. Groose, J. R. Holton, J. L. Lean, S. T. Massie, M. R. Schoeberl, A. R. Douglass, and C. H. Jackman (1998), Selected science highlights from the first five years of the Upper Atmosphere Research Satellite (UARS) program, *Rev. Geophys.*, *36*, 183–210.

Dessler, A. E., and S. C. Sherwood (2003), A model of HDO in the tropical tropopause layer, *Atmos. Chem. Phys.*, *3*, 2173–2181.

Duncan, B. N., R. V. Martin, A. C. Staudt, R. Yevich, and J. A. Logan (2003), Interannual and seasonal variability of biomass burning emissions constrained by satellite observations, *J. Geophys. Res.*, *108*(D2), 4100, doi:10.1029/2002JD002378.

Folkins, I., M. Loewenstein, J. Podolske, S. J. Oltmans, and M. Proffit (1999), A 14 km mixing barrier in the tropics: Evidence from ozonesondes and aircraft measurements, *J. Geophys. Res.*, *104*, 22,095–22,102.

Fueglistaler, S., H. Wernli, and T. Peter (2004), Tropical troposphere-to-stratosphere transport inferred from trajectory calculations, *J. Geophys. Res.*, *109*, D03108, doi:10.1029/2003JD004069.

Gettelman, A., M. L. Salby, and F. Sassi (2002a), Distribution and influence of convection in the tropical tropopause region, *J. Geophys. Res.*, *107*(D10), 4080, doi:10.1029/2001JD001048.

Gettelman, A., W. J. Randel, F. Wu, and S. T. Massie (2002b), Transport of water vapor in the tropical tropopause layer, *Geophys. Res. Lett.*, *29*(1), 1009, doi:10.1029/2001GL013818.

Gettelman, A., P. M. D. Forster, M. Fujiwara, Q. Fu, H. Vomel, L. K. Gohar, C. Johanson, and M. Ammerman (2004), Radiation balance of the tropical tropopause layer, *J. Geophys. Res.*, *109*, D07103, doi:10.1029/2003JD004190.

Gill, A. E. (1980), Some simple solutions for heat-induced tropical circulation, *Q. J. R. Meteorol. Soc.*, *106*, 447–462.

Holloway, C. E., and J. D. Neelin (2006), The convective cold top and quasi-equilibrium, *J. Atmos. Sci.*, in press.

Holton, J. R., and A. Gettelman (2001), Horizontal transport and the dehydration of the stratosphere, *Geophys. Res. Lett.*, *28*, 2799–2802.

Kalnay, E., et al. (1996), The NCEP/NCAR 40-year reanalysis project, *Bull. Am. Meteorol. Soc.*, *77*, 437–471.

Kiladis, G. N., K. H. Straub, and P. T. Haertel (2005), Zonal and vertical structure of the Madden-Julian oscillation, *J. Atmos. Sci.*, *62*, 2790–2809.

Kuang, Z., and C. S. Bretherton (2004), Convective influence on the heat budget of the tropical tropopause layer: A cloud-resolving model study, *J. Atmos. Sci.*, *61*, 2927–2929.

Liebmann, B., and C. A. Smith (1996), Description of a complete (interpolated) outgoing longwave radiation data set, *Bull. Am. Meteorol. Soc.*, *77*, 1275–1277.

Livesey, N. J., et al. (2005), EOS MLS version V1.5 level 2 data quality and description document, Jet Propul. Lab., Pasadena, Calif. (Available at http://mls.jpl.nasa.gov)

Madden, R. A., and P. R. Julian (1971), Description of a 40–50 day oscillation in the zonal wind in the tropical Pacific, *J. Atmos. Sci.*, *28*, 1109–1123.

Madden, R. A., and P. R. Julian (1972), Description of global scale circulation cells in the Tropics with a 40–50 day period, *J. Atmos. Sci.*, *29*, 1109–1123.

Madden, R. A., and P. R. Julian (1994), Observations of the 40–50 day tropical oscillation—A review, *Mon. Weather Rev.*, *122*, 814–837.

Mote, P. W., H. L. Clark, T. J. Dunkerton, R. S. Harwood, and H. C. Pumphrey (2000), Intraseasonal variations of water vapor in the tropical upper troposphere and tropopause region, *J. Geophys. Res.*, *105*, 17,457–17,470.

Pickering, K. E., et al. (1996), Convective transport of biomass burning emissions over Brazil during TRACE A, *J. Geophys. Res.*, *101*, 23,993–24,012.

Potter, B. E., and J. R. Holton (1995), The role of monsoon convection in the dehydration of the lower tropical stratosphere, *J. Atmos. Sci.*, *52*, 1034–1050.

Randel, W. J., F. Wu, and W. R. Rios (2003), Thermal variability of the tropical tropopause region derived from GPS/MET observations, *J. Geophys. Res.*, *108*(D1), 4024, doi:10.1029/2002JD002595.

Read, W. G., D. L. Wu, J. W. Waters, and H. C. Pumphrey (2004a), Dehydration in the tropical tropopause layer: Implications from the UARS Microwave Limb Sounder, *J. Geophys. Res.*, *109*, D06110, doi:10.1029/2003JD004056.

Read, W. G., D. L. Wu, J. W. Waters, and H. C. Pumphrey (2004b), A new 147–56 hPa water vapor product from the UARS Microwave Limb Sounder, *J. Geophys. Res.*, *109*, D06111, doi:10.1029/2003JD004336.

Sassi, F., M. Salby, H. C. Pumphrey, and W. G. Read (2002), Influence of the Madden-Julian Oscillation on upper tropospheric humidity, *J. Geophys. Res.*, *107*(D23), 4681, doi:10.1029/2001JD001331.

Schoeberl, M. R., B. N. Duncan, A. R. Douglass, J. Waters, N. Livesey, W. Read, and M. Filipiak (2006), The carbon monoxide tape recorder, *Geophys. Res. Lett.*, *33*, L12811, doi:10.1029/2006GL026178.

Sherwood, S. C., and A. E. Dessler (2000), On the control of stratosphere humidity, *Geophys. Res. Lett.*, *27*, 2513–2516.

Sherwood, S. C., and A. E. Dessler (2001), A model for transport across the tropical tropopause, *J. Atmos. Sci.*, *58*, 765–779.

Sherwood, S. C., and A. E. Dessler (2003), Convective mixing near the tropical tropopause: Insights from seasonal variations, *J. Atmos. Sci.*, *60*, 2674–2685.

Sherwood, S. C., T. Horinouchi, and H. A. Zeleznik (2003), Convective impact on temperatures observed near the tropical tropopause, *J. Atmos. Sci.*, *60*, 1847–1856.

Waugh, D. W. (2004), Impact of potential vorticity intrusion on subtropical upper tropospheric humidity, *J. Geophys. Res.*, *110*, D11305, doi:10.1029/2004JD005664.

Weare, B. C., and J. S. Nasstrom (1982), Examples of extended empirical orthogonal function analyses, *Mon. Weather Rev.*, *110*, 481–485.

Wu, W., A. E. Dessler, and G. R. North (2006), Analysis of the correlations between atmospheric boundary-layer and free-tropospheric temperatures in the tropics, *Geophys. Res. Lett.*, *33*, L20708, doi:10.1029/2006GL026708.

A. E. Dessler and S. Wong, Department of Atmospheric Sciences, Texas A&M University, College Station, TX, USA. (swong@ariel.met.tamu.edu)